CHAPTER IV
POLY(VINYLIDENE FLUORIDE-CO-HEXAFLUOROPROPYLENE) /MICROCRYSTALLINE CELLULOSE (PVDF-HFP/MCC) COMPOSITE FILM

4.1 Abstract

Poly(vinylidene fluoride-co-Hexafluoropropylene) (PVDF-HFP) composites were fabricated via twin screw extruder to achieve the high dielectric and piezoelectric properties and also utilized as a touch sensor. This chapter, extracted microcrystalline cellulose (MCC) from sugarcane bagasses in 1-20 wt.% were provided as an appropriate filler to improve the dipole alignment of PVDF-HFP matrix. The cast film extruder was used to produce the transparent composite films with unique properties. The increment in β-phase crystalline presented with higher amount of BC. The dielectric constant corresponded to piezoelectric coefficient was enhanced from 2.00 of neat PVDF-HFP to 3.25 with 5 wt.% BC loading. Besides, the presence of BC in the composite films leaded to an improvement in thermal properties, and mechanical properties in terms of Young's modulus and tensile strength with no dimensional changes at 110 °C due to the excellent thermal, and mechanical properties of BC structure.

4.2 Introduction

Films of some polymers, such as polyvinylidene fluoride (PVDF) and its copolymers,opportunely conditioned, exhibit piezoelectric and pyroelectric properties [1–6] with excellent sensitivity and a satisfactory dynamic response. Moreover, they can be reduced to tiny compliant strips for embedding in a continuous elastic layer. Used as isolated sensors/actuators or assembled into more complex multimodal devices, they offer challenging solutions in many application fields including robotics. For these reasons they can be regarded as interesting candidates for touch sensors or touch screen panel [7]. PVDF is synthesized by addition polymerization of the CH2 CF2 monomer. When produced as the homopolymer (i.e. from 100% CH2 CF2 monomer), the majority of the PVDF chains have a regular structure of alternating

CH2 and CF2 groups. The crystalline phase of interest for PVDF ferroelectricity is the polar β-phase. This structure can be obtained either by using the PVDF trifluoroethylene copolymer [P(VDF-TrFE)] which has the tendency to crystallize directly in the polar β -phase or by mechanical stretching of ofthe α -phase [9-12], from melt under specific conditions such as high pressure [13], external electric field [14] and ultra-fast cooling [15].

However, there is a need to develop a touch sensor with high mechanical properties for their long term operation and tolerance to the applied force during electronic device lifetime. Up to the present time, in order to fulfill flexible characteristic and maintain the excellence on dimensional stability, one of the materials found to be promising was transparent cellulose composite. Cellulose is a interesting material because of its abundant availability, biodegradability, and low cost [16]. The use of cellulose also generally provides numerous advantages including biodegradability, light weight, transparency, including high strength. Cellulose is typically separated from lingocellulosic plants, such as wood and agricultural crops, using mechanical treatment. Usually, lignin is also removed from the plant cell wall prior to fibrillation using chemical treatment [17].

Due to the fact that cellulose is hydrophilic and forms irreversible aggregates when it dried, the most successful methods used to prepare the cellulose composites have been solution casting of dilute slurry of matrix and cellulose [18]. However, for larger scale production these methods are slow and expensive. Extrusion compounding is one of the most promising methods for industrial processing due to easy scale-up and the possibility of further molding of the materials. It also tends to reduce environmental hazards. There are only few published studies on extrusion processing of cellulose composites which is why more research is needed.

The objective of this work is to develop the transparent and flexible touch sensor based on piezoelectric material for touch screen applications. We used microcrystalline cellulose (MCC), extracted from sugarcane bagasses, as a filler to improve the dipole alignment of PVDF-HFP matrix by using melt mixing method followed by cast film process. The dielectric constant was measured as the electrical and piezoelectric properties. In addition, the morphological, thermal and mechanical

properties were analyzed and discussed based on basis properties for touch screen applications.

4.3 Experimental

4.3.1 Materials

Poly(vinylidene fluoride-co-Hexafluoropropylene) or PVDF-HFP with a melt flow rate of 7 g/10 min (5 kg at 230°C), Solef® 1010/1001 from Solvay was purchased from Prostar Chemicals Co., Ltd., Thailand.; Bagasse flour was purchased from local food market; Hydrochloric acid (HCl) was purchased from RCI labscan Co..Ltd.; Hydrogen peroxide (H_2O_2) was purchased from Chem-Supply Pty Ltd.: Sodium hydroxide (NaOH) (AR grade, 98%) were purchased from Merck Ltd.

4.3.2 Methods

4.3.2.1 Microcrystalline Cellulose (MCC) preparation

Following the previous work of Thiangtham (2014), first, the bagasse flour was delignified using alkaline peroxide solution. The dried bagasse was treated with 10% (w/v) sodium hydroxide (NaOH) at 80°C for 4 hours to removed hemicellulose and lignin. The residue was washed with distilled water to remove NaOH. Then the delignified bagasse flour was bleached with10% (v/v) hydrogen peroxide (H_2O_2) at 80°C for an hour until the wood became white. Second, the bleached wood flour was treated in 4M hydrochloric acid (HCl) at 80°C for an hour to hydrolyze to reach nano-sized. At the end of the extraction, the residue was continuously washed thoroughly with distilled water until neutral. The resulting cellulose was dried at 60°C for 2 days. Then, the dry cellulose was sieved to produce uniform powder with size less than 74 μm and defined as MCC.

4.3.2.2 PVDF-HFP/MCC composite film preparation

All materials were generously pre-compounded and pelletized using a co-rotating twin-screw extruder (LTE-20-40 Lab Tech). The PVDF-HFP pellets and MCC powders were dried at 60°C for 48 hours prior to remove adsorbing water. The amount of blends prepared was 1 kg per each blend ratio, depending on main polymer. Pre-mixtures of PVDF-HFP with MCC with the dry

weight ratio between PVDF-HFP:MCC varied at 1000:0, 99:1, 97:3, 95:5, 90:10, and 80:20 % by weight were blended in a laboratory blender to form uniform powder. The amount of materials prepared of each blend ratio was reported in Table 4.1.

Table 4.1 Amount of materials prepared for each blend ratio

Formula	PVDF-HFP (g)	MCC (g)
PVDF-HFP	1000	-
PVDF-HFP/MCC (1 wt.%)	990	10
PVDF-HFP/MCC (3 wt.%)	970	30
PVDF-HFP/MCC (5 wt.%)	950	50
PVDF-HFP/MCC (10 wt.%)	900	100
PVDF-HFP/MCC (20 wt.%)	800	200

PVDF-HFP/MCC composites were melted mixing in a twin screw extruder. The processing temperature, residence time and the screw speed were maintained at 150-160-165-170-175°C, 10 min and 30 rpm, respectively. The extruder barrel was equipped with two atmospheric vents and vacuum ventilation in purpose to remove the vaporized water from the material.

After pelletizing, the PVDF-HFP and its composite pellets were dried at 60°C for 48 hours before film casting process to prepare the thin film. The temperatures of the extruder were set at 170-180°C. The screw speed for the samples was 65 rpm. The die temperature was fixed at 180°C. The chill roll was placed in 2 cm from the die and its temperature was kept at 20°C by temperature controller. The film was quenched by a chill roll and was transported to a pulling station using a nip roll. The speed of chill and nip rolls were controlled separately from the extruder using a dial and digital display. As reference, the neat PVDF-HFP film was also prepared in similar manner.

4.4 Results and Discussions

4.4.1 Microcrystalline Cellulose (MCC) Characterization

4.4.1.1 Morphological Properties

Figure 4.1 shows the visual appearance and SEM images of MCC. The MCC displays irregular shape and apparent size dispersion. The particles sizes were in the range of 30-70 μm.

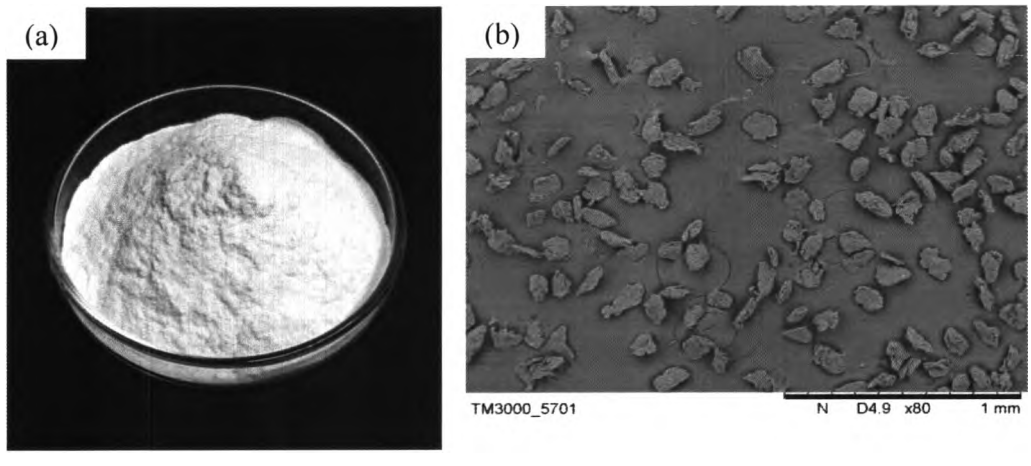

Figure 4.1 (a) The visual appearance and (b) SEM image of MCC.

4.4.1.2 Crystallinity

XRD diffractogram of MCC is shown in Figure 4.2. The result shows three main diffraction peaks at 2θ of 16.5°, 22.5°, and 35.0° which refer to the 110, 020, and 004 diffraction planes, respectively. These diffractions correspond to the typical profile of the cellulose I allomorph [17-18]. The crystallinity of MCC is 58% which was calculated based on crystalline peak, due to the acid treatment, as the acid preferably hydrolyzed the amorphous and less-ordered regions of bagasses [19].

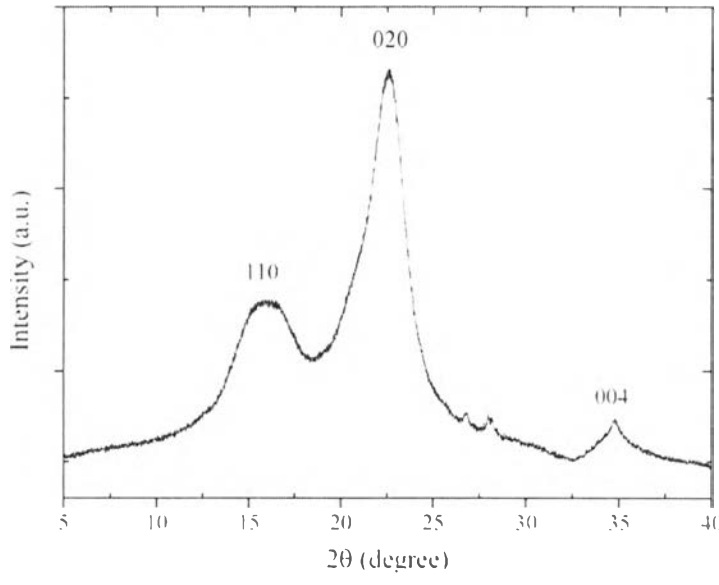

Figure 4.2 XRD diffractogram of MCC.

4.4.1.3 Chemical Properties

The FT-IR spectra of MCC is shown in Figure 4.3. The structure of MCC is linear homopolymer composed of D-glucopuranose units linked by β-1,4-glycosidic linkage at C_1 and C_4 carbon position [20]. The peak at 3332 cm^{-1} referred to O-H stretching vibration, while the peak at 2893 cm^{-1} and 1429 cm^{-1} referred to C-H stretching and symmetric blending of $-CH_2$, respectively. The peak at 897 cm^{-1} indicated to C-O stretching [21]. The peaks at 1429, 1110, and 897 cm^{-1} were thought to be the typical bonds of cellulose I (Iβ) [18], which was consistent with XRD diffractogram.

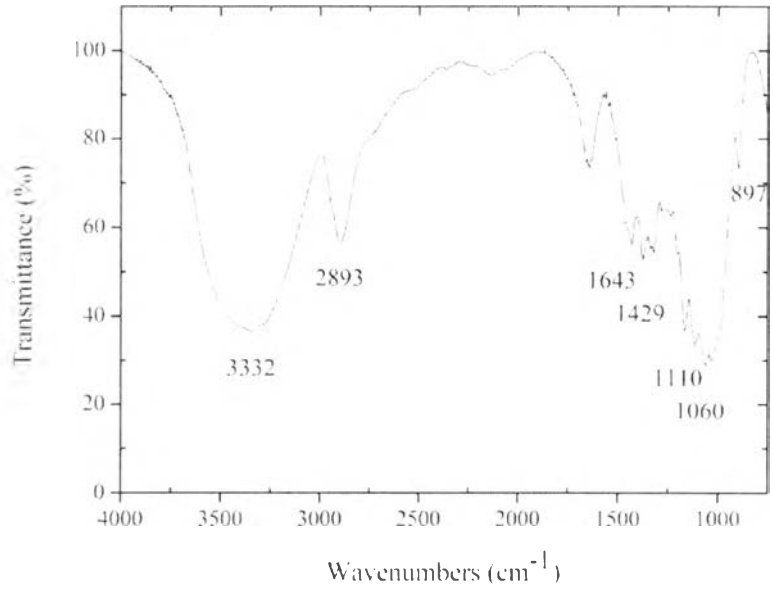

Figure 4.3 FT-IR Spectra of MCC.

4.4.1.4 Thermal Properties

TGA thermogram of the MCC (a) and its derivative peak (b) are shown in Figure 4.4. There are two thermal degradation steps corresponding to the vaporization of adsorbed water in the MCC (start from 40°C) and the degradation process such as depolymerization, dehydration and carbonization of MCC chain (start from 300 °C). The degradation temperature (T_d) of MCC was 322°C. When temperature reaches 400 °C the formation of charred residue is occured and its remaining weight was evaluated at approximately 10% referring to char residue [22].

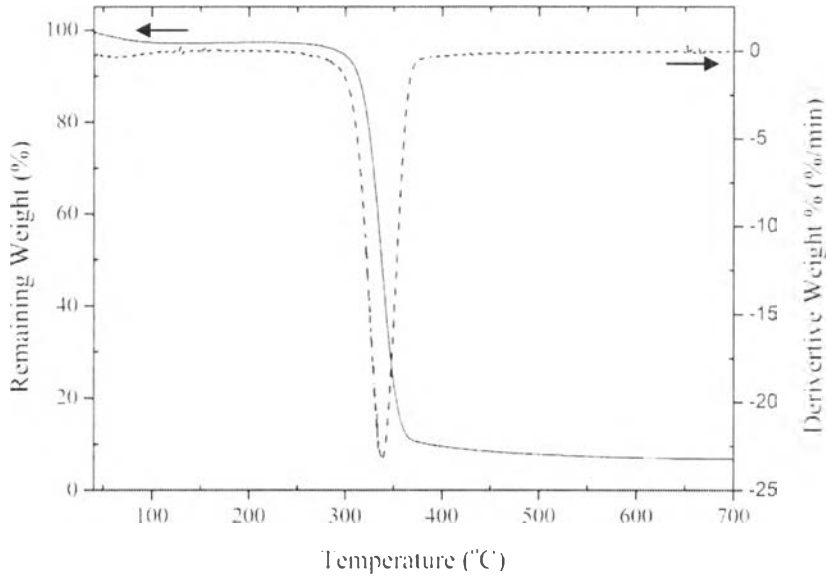

Figure 4.4 TGA thermogram of MCC (—) and its derivative (---).

4.4.2 PVDF-HFP and PVDF-HFP/MCC Films Characterization

4.4.2.1 Morphological Properties

Extruded pellet and casted films with a thickness ranging between 0.1 and 0.2 mm are shown in Figure 4.5. Both of neat PVDF-HFP pellet and casted film were transparency. After mixing, the composite pellets and films were yellow which could be due to the degradation process of the residual lignin which is a consequence of alterations in the physiological and biochemical processes and has resulted in yellow color of the matrix [23]. In addition, the neat PVDF-HFP film was more transparent than the composites in agreements with observations reported previously by Fortunati (2010) [24]. This optical result can be confirmed by UV/Vis spectra by using air as reference (Figure 4.6). Neat PVDF-HFP film has 50-70% transmittance in the visible light region (400-750 nm), but when adding MCC, the transmittance tends to decrease, which means MCC exhibits the opacity property. It is due to the formation of a network structure in the MCC. It can be suggested that with high amount of MCC may segregate from the blend to form a micro-sized aggregation which can be observed in the visible light region. Similar to Auras's work, MCC show a blocking effect on the ultra violet C region (280–100 nm), usually produced by artificial light sources [25].

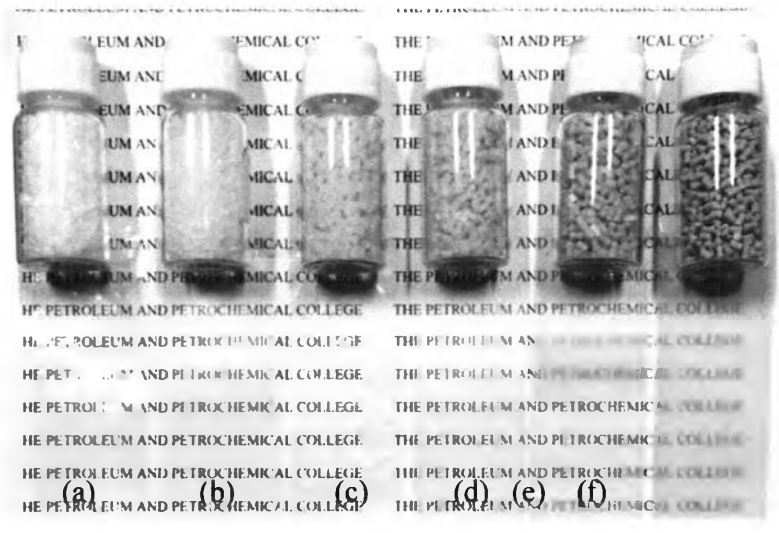

Figure 4.5 The visual appearance of extruded pellet and casted film of (a) PVDF-HFP, (b) PVDF-HFP/MCC (1 wt.%), (c) PVDF-HFP/MCC (3 wt.%), (d) PVDF-HFP/MCC (5 wt.%), (e) PVDF-HFP/MCC (10 wt.%), and (f) PVDF-HFP/MCC (20 wt.%).

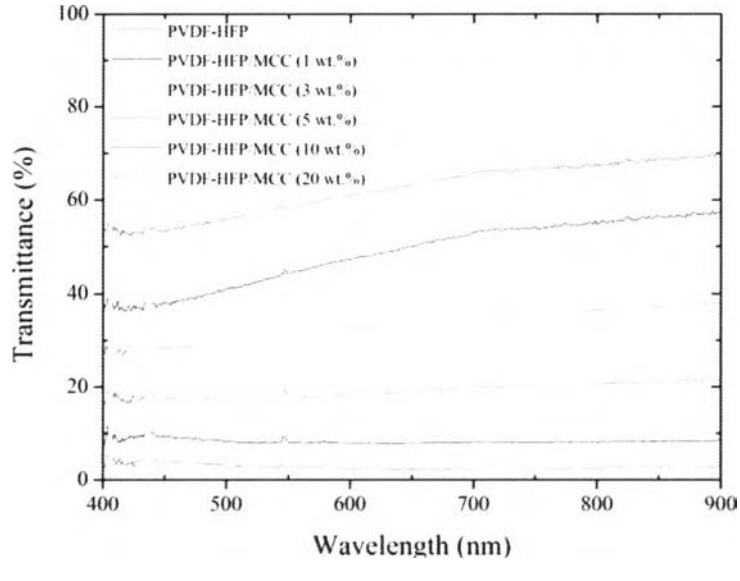

Figure 4.6 The UV/Vis spectra of neat PVDF-HFP and PVDF-HFP/MCC composite films.

Morphological aspects of the cross-section of neat PVDF-HFP and PVDF-HFP/MCC (3 wt. %) composite film were investigated by FE-SEM and the images are shown in Figure 4.7. The neat PVDF-HFP film (Figure 4.7a) shows a typical smooth and uni-form surface of polymer, while PVDF-HFP/MCC composite film (Figure 4.7 b) show some compact structures (arrows), suggesting that MCC are present in flakes [26]. It was clearly indicated that adding of BC caused an increasing of roughness of film.

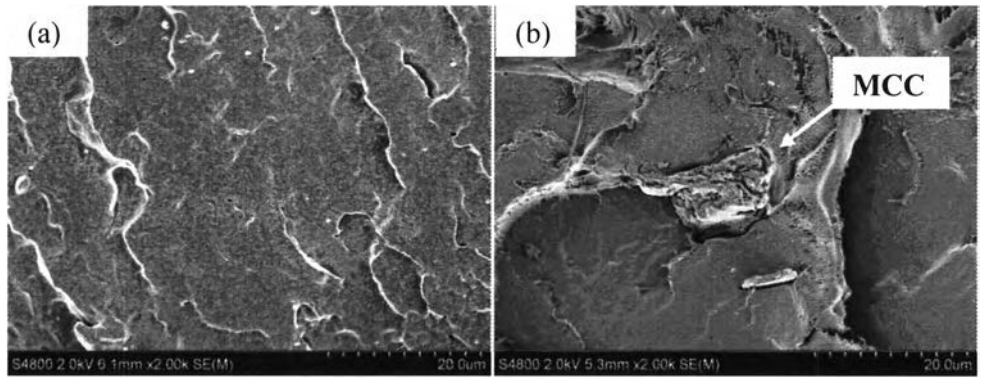

Figure 4.7 The SEM images of cross-section surface of (a) PVDF-HFP and (b) PVDF-HFP/MCC (3 wt.%)

The dispersion of MCC particles in the PVDF-HFP matrix were observed by an optical microscope. Figure 4.8 shows the optical microscope images. At low contents of 1-3 wt.% (Figure 4.8b-c), most MCC particles dispersed uniformly in the PVDF-HFP matrix without agglomeration and obtain a good orientation in machine direction. While the aggregation of MCC particles increased with an increasing MCC content (Figure 4.8d-f).

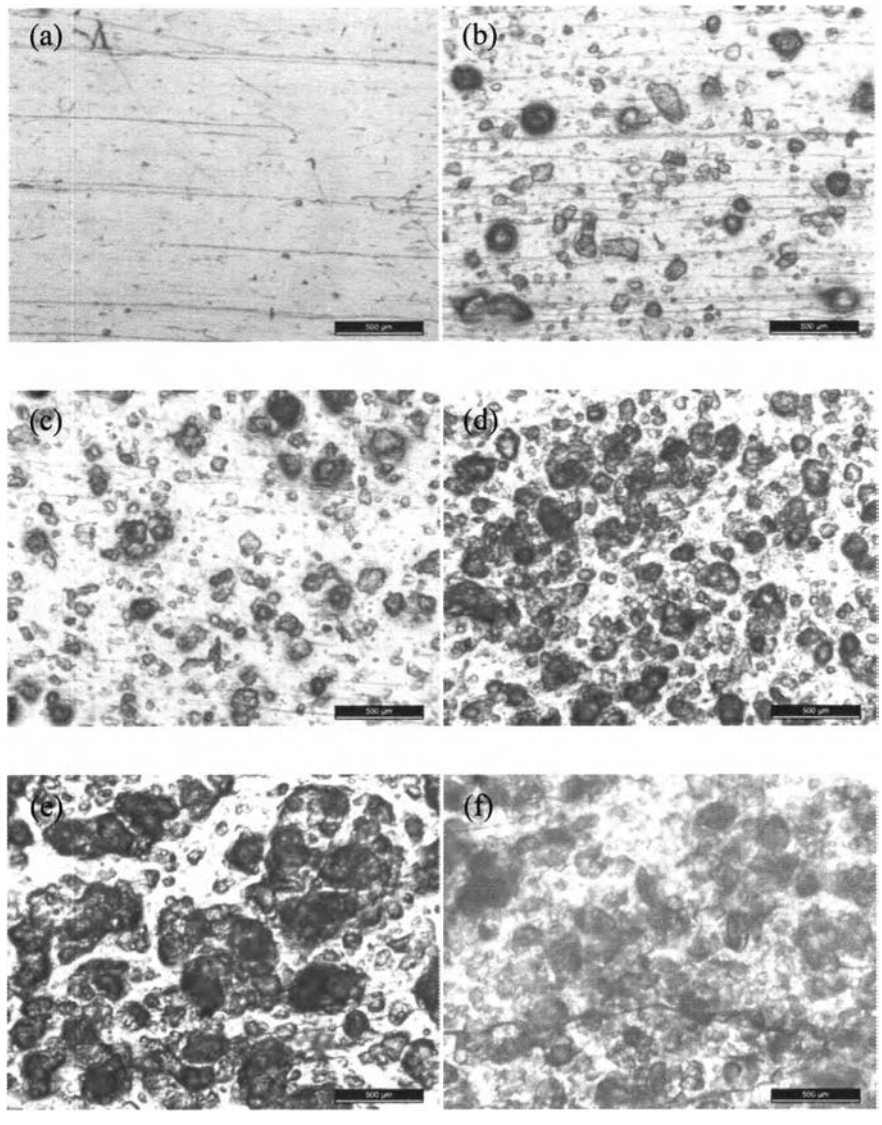

Figure 4.8 The Optical microscope images of (a) PVDF-HFP, (b) PVDF-HFP/MCC (1 wt.%), (c) PVDF-HFP/MCC (3 wt.%), (d) PVDF-HFP/MCC (5 wt.%), (e) PVDF-HFP/MCC (10 wt.%), and (f) PVDF-HFP/MCC (20 wt.%).

4.4.2.2 Crystallinity

PVDF, the main constituent of the PVDF-HFP copolymer used in this work as polymer host, can present several different crystalline structures.

In general, the functional group of PVDF ($-CH_2-CF_2-$) exist five molecular conformations (α, β, δ, γ, and ε). The α and β-phases are commonly studied and also the most important polymorphs for PVDF and its copolymers.

The absorption bands characteristic of neat PVDF-HFP and PVDF-HFP/MCC composite films was shown in Figure 4.9. The basic characteristic absorption peaks of PVDF-HFP, *i.e.* CH_2 wagging, antisymmetric CF_2 stretch, and CF_3 out-of-plane deformation absorb IR radiation at 1402, 1180 and 1065 cm^{-1} [26-27], respectively. Moreover, the absorption band of α-phase, which is a non-polar trans-gauche-trans- gauche' (TGTG') conformation, were observed at 763 cm^{-1} (CF_2 bending), and 795 cm^{-1} (CF_2 rocking). While the presence of β-phase, all-trans (TTTT) or planar zigzag conformations observed by the specific absorption bands at 840 and 1285 cm^{-1} (CH_2 rocking and bending, respectively) [26-29]. While the amorphous region, which was observed at 873 cm^{-1}, come from the HFP phase of PVDF-HFP.

According to Equation 3.2, the fraction of β-phase, $F(\beta)$, was calculated from FTIR spectra and presented in Table 4.2, assuming that there is no absorbance contribution from the MCC. With the higher amount of MCC incorporated, β phase tends to be increased because crystallization was obstructed by the network of MCC. The β-phase content for neat PVDF-HFP film is 47% and increase with increasing MCC content. This result indicated that the introduction of MCC probably acting as a nucleation site led to a change of the crystalline phase from α to β phase crystals. It is implied that the introduction of MCC in PVDF-HFP matrix at high content prohibits the transformation from α to β-phase. For the mechanisms of the phase transformation in the PVDF-HFP composites, it is reasonable to believe that the efficiency of the phase transformation is related to the interfacial areas between filler and PVDF-HFP matrix [29]. Therefore the phase transformation is limited by the small interfacial area when the content of MCC is high and tent to agglomerate (see Figure 4.8f). As the concentration of MCC is lower than 20 wt.% , a greater number of interfaces between PVDF-HFP and MCC are formed due to the good MCC dispersion (see Figure 4.8a-e).

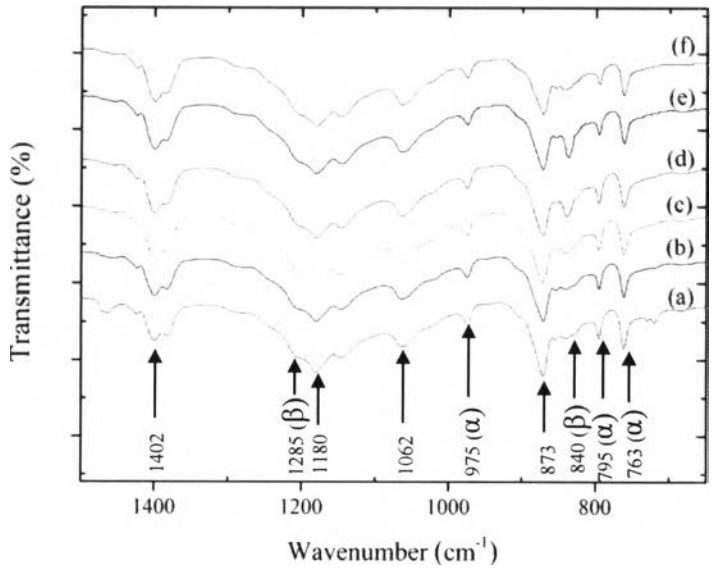

Figure 4.9 FT-IR spectra of (a) PVDF-HFP, (b) PVDF-HFP/MCC (1 wt.%), (c) PVDF-HFP/MCC (3 wt.%), (d) PVDF-HFP/MCC (5 wt.%), (e) PVDF-HFP/MCC (10 wt.%), and (f) PVDF-HFP/MCC (20 wt.%).

Table 4.2 β-phase fraction; F(β), of neat PVDF-HFP and its composite films

Formula	F(β)
PVDF-HFP	0.47
PVDF-HFP/MCC (1 wt.%)	0.47
PVDF-HFP/MCC (3 wt.%)	0.49
PVDF-HFP/MCC (5 wt.%)	0.50
PVDF-HFP/MCC (10 wt.%)	0.50
PVDF-HFP/MCC (20 wt.%)	0.47

To confirm the presence of β-phase in PVDF-HFP/MCC composites, XRD analysis was also used to investigate. Figure 4.10 shows XRD patterns of crystalline phase of PVDF-HFP and its composite films with 1, 3, 5, 10, and 20 wt.% of MCC loading. Similar to Chang's work [29], there were two characteris-

tic peaks which refers to α and β-phases. In our study, the characteristic peaks at 17.5°, 17.9°, 20.0°, and 27.0° corresponding to monoclinic α phase ofα(0 2 0), α(1 0 0), α(1 1 0), and α(0 2 1), respectively [28]. In the case of PVDF-HFP/MCC composites, a new reflection peak at 2θ = 20.4°corresponding to β phase, which has orthorhombic unit cell, appeared, and the peak intensity increased with increasing MCC content which was corresponded to the FT-IR result. This result indicated that the introduction of MCC probably acting as a nucleation site led to a change of the crystalline phase from α to β phase crystals. As well documented in literature [22-30], α-form crystal is non polar phase (trans-gauche-trans-gauche' (TGTG'), while β-form crystal shows polar properties. Therefore, it can be inferred that the polarity of the materials increased as the content of MCC increasing.

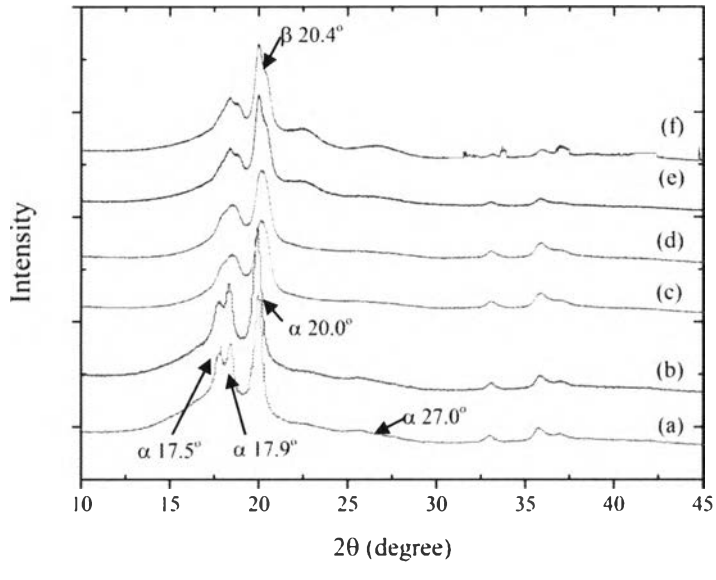

Figure 4.10 XRD patterns of (a) PVDF-HFP, (b) PVDF-HFP/MCC (1 wt.%), (c) PVDF-HFP/MCC (3 wt.%) , (d) PVDF-HFP/MCC (5 wt.%), (e) PVDF-HFP/MCC (10 wt.%), and (f) PVDF-HFP/MCC (20 wt.%).

4.4.2.3 Thermal Properties

In order to determine the thermal behavior of the neat PVDF-HFP and PVDF-HFP/MCC composite film, DSC studies were carried out. The DSC

parameters are shown in Table 4.3. From the result, there are transition temperature peaks observed at about 160 °C and 120 °C which corresponding to T_m and T_c of PVDF-HFP, respectively.

Figure 4.11 shows the second-heating curves of neat PVDF-HFP and its composite films. The inclusion of MCC in polymer matrix shows slightly effects on T_m of PVDF-HFP matrix. The increase in the T_m value was due to the higher thermal stability of MCC and the interaction between oxygen atoms of MCC with hydrogen atoms of PVDF-HFP, while fluorine atoms in PVDF-HFP may also be attracted to hydrogen atoms in MCC [35].

Exothermic peaks of crystallinity temperature are shown in Figure 4.12 indicate that higher amount of MCC shift T_c to higher temperature because the composite films need higher energy to crystallize with the presence of MCC.

Furthermore, the degree of crystallinity (X_c) will be measured as the ratio between ΔH_m and ΔH_m^0, as equation 3.2. As shown in Table 4.3, the increasing of MCC causes slight decrement of X_c from 55.5 to 53.0. It can be described that the PVDF-HFP crystallization process may be disturbed by the micro structure of MCC. Conclusively, although the MCC induced the crystal transformation from α to β form, it reduced the crystallinity of PVDF-HFP. It is also reported in other literature that the reduced crystallinity occurred during the phase transformation [36-37]. An explanation for this phenomenon is that the fusion and incomplete recrystallization of the crystal phase in semi-crystalline PVDF-HFP was the cause of the reduced crystallinity [37].

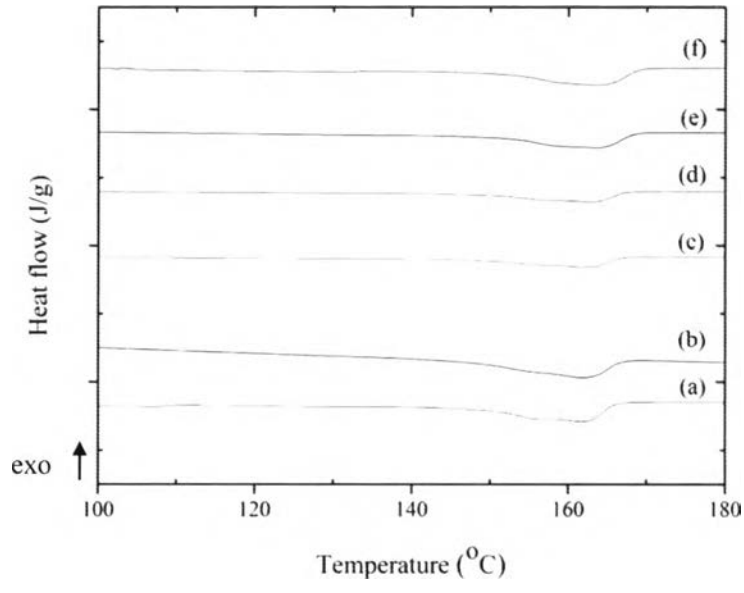

Figure 4.11 DSC second-heating curves of (a) PVDF-HFP, (b) PVDF-HFP/MCC (1 wt.%), (c) PVDF-HFP/MCC (3 wt.%), (d) PVDF-HFP/MCC (5 wt.%), (e) PVDF-HFP/MCC (10 wt.%), and (f) PVDF-HFP/MCC (20 wt.%).

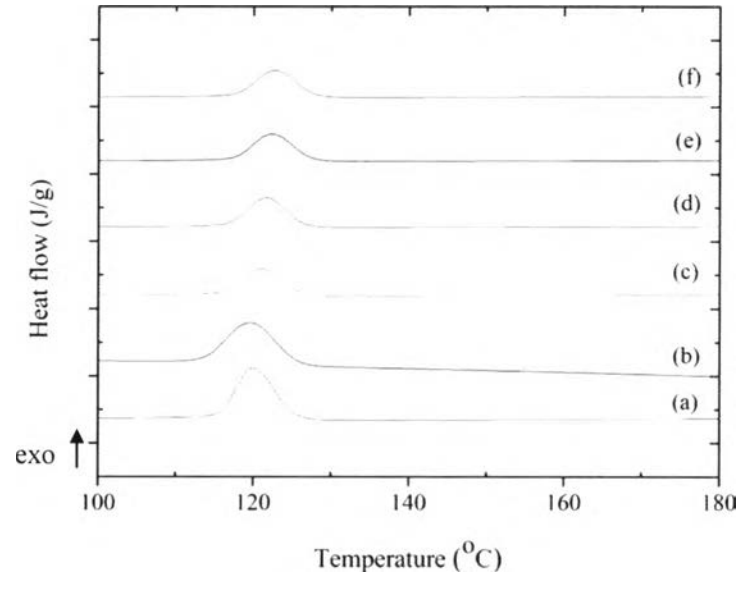

Figure 4.12 DSC first-cooling curves of (a) PVDF-HFP, (b) PVDF-HFP/MCC (1 wt.%), (c) PVDF-HFP/MCC (3 wt.%), (d) PVDF-HFP/MCC (5 wt.%), (e) PVDF-HFP/MCC (10 wt.%), and (f) PVDF-HFP/MCC (20 wt.%).

Table 4.3 DSC parameters of neat PVDF-HFP and its composite films

Formula	T_m[a] (°C)	T_c[b] (°C)	ΔH_m[c] (J/g)	X_c[d] (%)
PVDF-HFP	161.6	120.0	57.5	55.5
PVDF-HFP/MCC (1 wt.%)	161.3	119.7	59.1	57.0
PVDF-HFP/MCC (3 wt.%)	162.3	121.3	56.8	54.8
PVDF-HFP/MCC (5 wt.%)	162.6	121.6	55.0	53.0
PVDF-HFP/MCC (10 wt.%)	163.3	122.3	55.2	52.7
PVDF-HFP/MCC (20 wt.%)	163.7	122.6	53.9	51.0

a is melting peak temperature, b is cooling peak temperature, c is melting enthalpy, and d is Crystallinity of PVDF-HFP

Note: Crystallinity of PVDF-HFP was calculated by using the data on heating process.

Thermal degradation behavior was observed by using TGA. Figure 4.13 showed TGA thermograms of MCC, neat PVDF-HFP, and its composite films. It was found that the thermal degradation behavior of the PVDF-HFP/MCC composite films was divided into two steps. The first step started at 300 °C, which corresponded to the degradation temperature of MCC (see Figure 4.4) [31]. Where, the degradation of second step started at 420 °C, which corresponded to the degradation temperature of PVDF-HFP matrix [32]. The degradation temperature of PVDF-HFP matrix was not affected by the dispersion of MCC. When temperature reaches 550 °C, the formation of char residue is presented. The degradation temperature are shown in table 4.4.

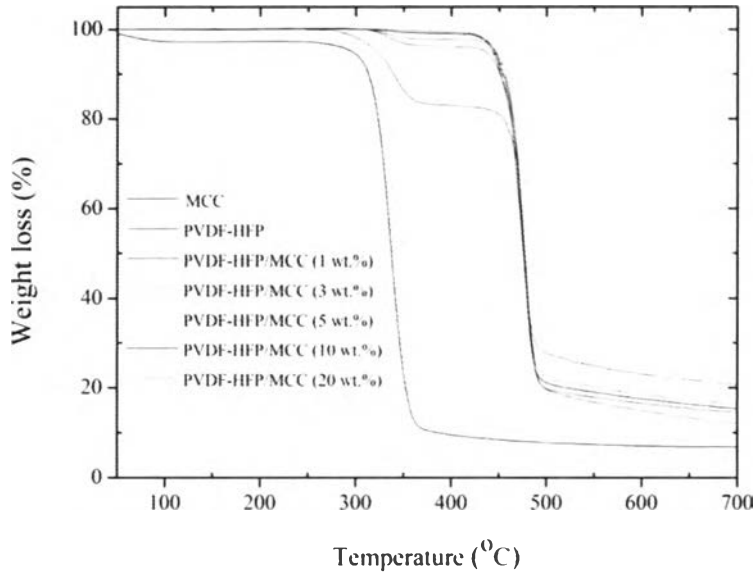

Figure 4.13 TGA thermograms of neat PVDF-HFP and its composite films.

Table 4.4 The degradation temperature (T_d) and char residue of PVDF-HFP and its composite films

Formula	T_{d1}(°C)		T_{d2}(°C)	
	onset	peak	onset	peak
PVDF-HFP	-	-	421	475
PVDF-HFP /MCC (1 wt.%)	-	-	421	476
PVDF-HFP/MCC (3 wt.%)	310	340	424	477
PVDF-HFP/MCC (5 wt.%)	310	341	422	477
PVDF-HFP/MCC (10 wt.%)	302	338	422	476
PVDF-HFP/MCC (20 wt.%)	300	335	424	475

4.4.2.4 Dielectric Properties

The frequency dependence at 20°C of the dielectric constant at low and high frequency range of the films were shown in Figure 4.14 (a) and 4.15 (a), respectively. The decrease in dielectric constant with increasing frequency could be explained on the basis of dipole relaxation phenomenon. At low frequency, the

dipoles in polymeric chain had sufficient time to align with the electrical field direction causing the higher dielectric constant and the inability of the electric dipoles to be in pace with the frequency of applied electric field at high frequency. It can be concluded that the dielectric behaviors of the PVDF-HFP and it composite film strongly depend on the variation of frequency. Dielectric constant of the composites slightly increases with increasing MCC content up to 10 wt.%, after that dielectric constant was found to decrease when adding the MCC up to 20 wt.% which correspond to β-phase content (Table 4.2). The highest dielectric constant value of PVDF-HFP composite was observed at 1 kHz when the content of MCC was added 10 wt.%.

Figure 4.14(b) and 4.15(b) showed the frequency dependence of the dissipation factor at low and high frequency regions of all samples. It was observed that the dielectric loss increased as frequency increased for both neat PVDF-HFP and PVDF-HFP/MCC composite films at low frequency (from 1 kHz to 1 MHz), but decreased as frequency increased at high frequency up to 1 GHz, the upper limit of the frequency range in this study. The maximum value of dielectric loss is reached at the frequency of 1 MHz.

Figure 4.16 exhibits the temperature dependence of the dielectric constant and dissipation factor was at 2-5 and 0.02-0.20, respectively at wide range of temperature and frequency range from 10 MHz to 1 GHz. At constant frequency with high temperature, the dielectric constant tended to be high due to polymer chains can be free to vibrate, move and reorient which allowing them to keep up with the changing electric field. When the successfully orientation was obtained, the dielectric constant became constant. With lower temperature, the segmental motion of the chain is practically frozen when the temperature was much lower than dynamic T_g which causing the lower dielectric constant [33]. Moreover, the result showed that dielectric constant was increase as increasing MCC content, and decrease when the MCC content up to 20 wt.% which correspond to the result from previous paragraph. The dielectric relaxation mechanism of neat PVDF-HFP and composite films can be observed in Figure 4.16 (right), it was found that there's only one relaxation mechanism appeared which was referred to the dynamic glass transition temperature (T_g) or the β relaxation that can be obtained by the dielectric response at very low

tion peak shifted to higher temperature (20 °C to 60 °C) because of polymeric chains in amorphous region has not enough energy to relax due to the very short time to store the energy, so the higher energy was needed for the chains to vibrate and reorient along the electrical field. For the PVDF-HFP/MCC composite films, there's only one relaxation mechanism, which means that the incorporation of MCC didn't have the effect on the relaxation behavior of the blend films.

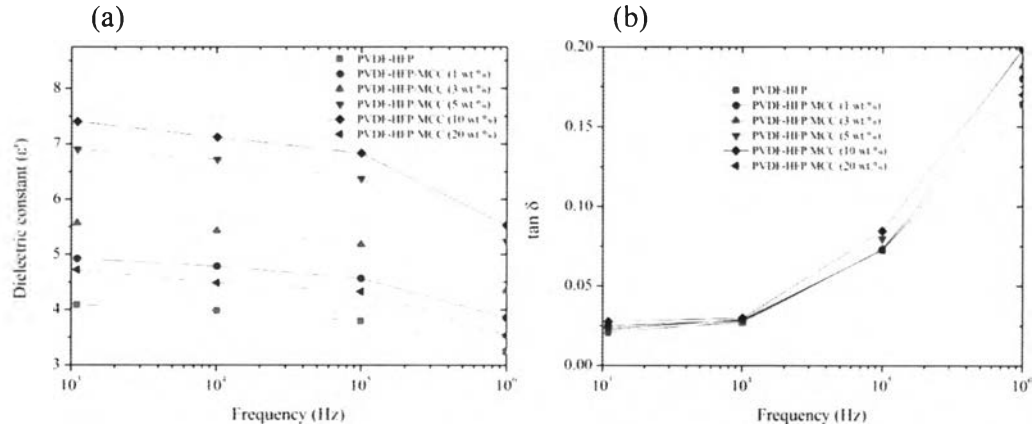

Figure 4.14 The frequency dependence of dielectric constant (a) and dissipation factor (b) of PVDF-HFP and its composite films at low frequency (1kHz-1MHz)(T = 20 °C)

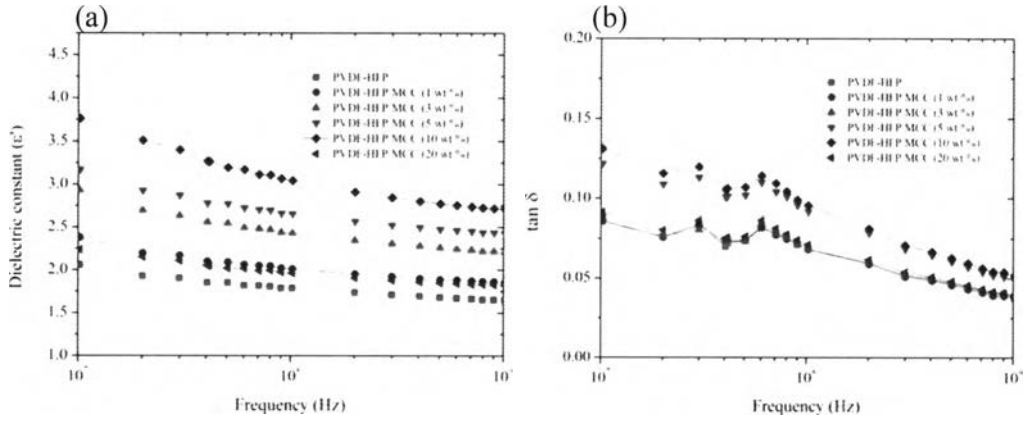

Figure 4.15 The frequency dependence of dielectric constant (a) and dissipation factor (b) of PVDF-HFP and its composite films at high frequency (10MHz-1GHz) (T = 20 °C).

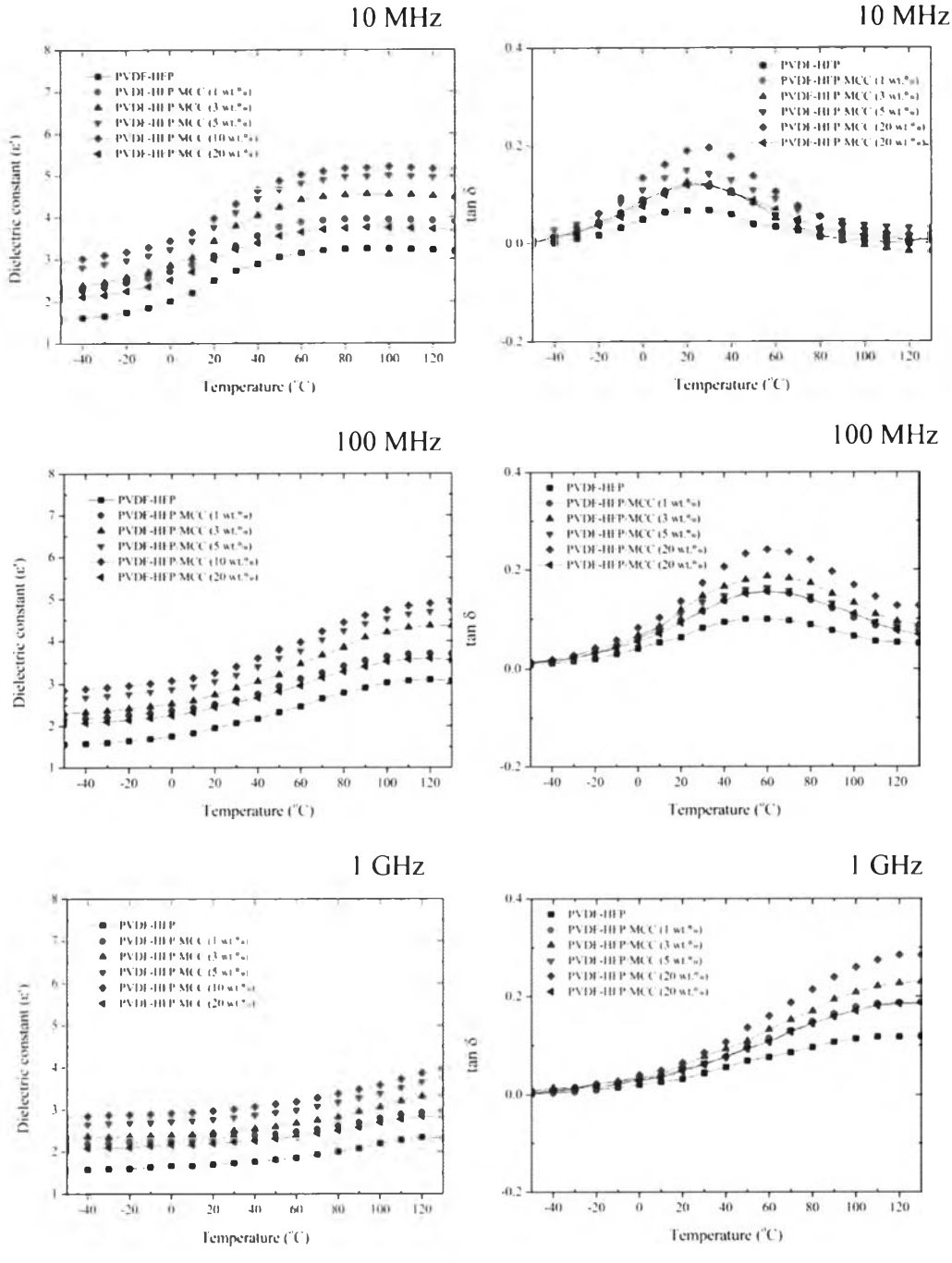

Figure 4.16 The temperature dependence of dielectric constant (left) and dissipation factor (right) of PVDF-HFP and its composite films (-50 °C - 130 °C) at frequency 10 MHz, 100 MHz, and 1 GHz.

Figure 4.17, shown the dielectric constant and dissipation factor at 10 MHZ as a function of MCC content, it can be seen that incorporation with higher amount of MCC exhibited significantly higher dielectric constant and dissipation factor. This increasing occurred due to the interfacial polarization between the hydroxyl group in the MCC chain and fluorine atom in PVDF-HFP chain. Moreover, as the particle size is in micrometer order, the number of particles per unit volume is large, hence the dipole moment per unit volume increases, and also the dielectric constant increases [35]. However, higher amounts of MCC, more free space occurred from repulsive force between the hydroxyl groups, and it consequently decreased the polarization, resulted in increasing on the dissipation factor. Moreover, a higher content of MCC in the composite film caused higher water content, which increased the loss of the composite films due to lower stability of the PVDF-HFP structure and a higher dissipation factor from the water [30]. It can be inferred that the 10 wt.% MCC is a critical filler concentration in PVDF-HFP/MCC composites film.

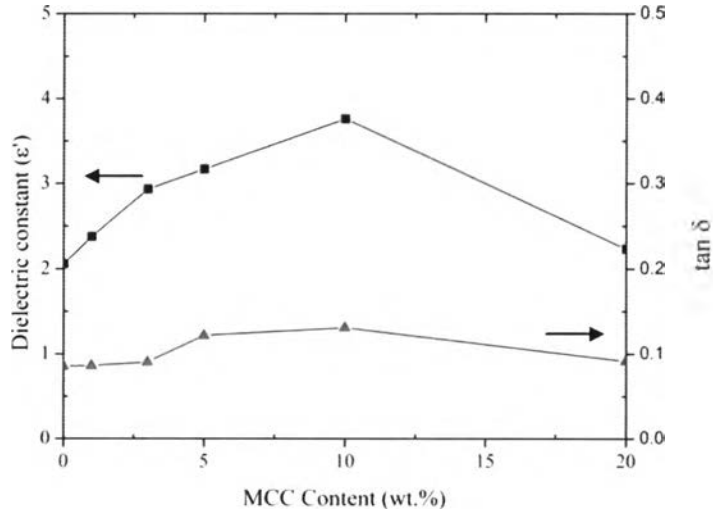

Figure 4.17 Dielectric constant and dissipation factor of PVDF-HFP and its composite films as a function of MCC content measured (10 MHz) at 20 °C.

4.4.2.5 Mixture of dielectrics

Figure 4.18 shows the typical experimental and theoretical dielectric permittivities of the PVDF-HFP/MCC composite films as a function of MCC content; Maxwell (equation 3.6), and log (equation 3.7) mixing rule. It can be seen here that dielectric constant measurement was always greater than theories. From experimental, the dielectric constant increase with increasing MCC content up to 10 wt.%, and with further MCC increase up to 20 wt.% the dielectric constant decreased. It was also observed that the results of the Maxwell and log mixing rule calculations were very different from the experimental results in this frequency range. These theories are based on a spherical morphology of the filler particles. Due to the non-spherical morphology of the MCC (see Figure 4.1), the theoretical calculations of the dielectric constant were not completely in accord with the experimental results. In this case, the results showed that the Maxwell and log mixing rule were not suitable theory for calculating the dielectric constant of the PVDF-HFP/MCC composite films which prepared by melt process.

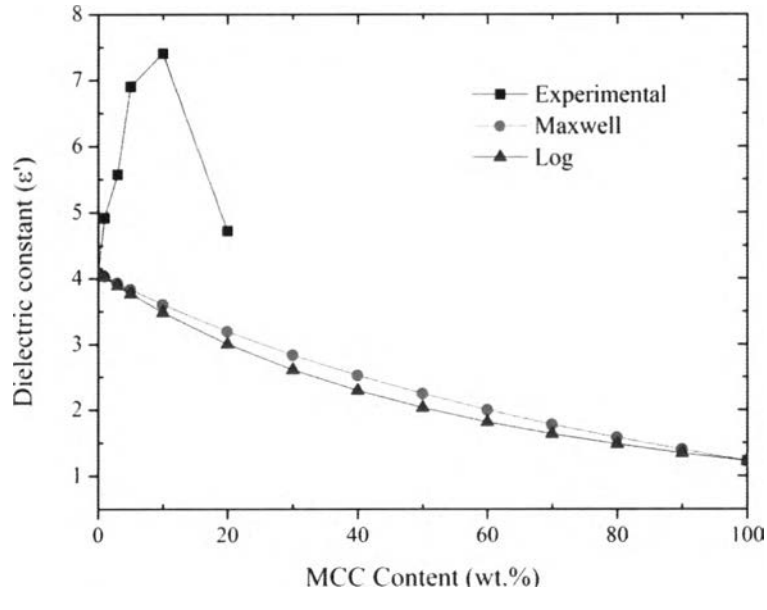

Figure 4.18 Dielectric constant of PVDF-HFP/MCC composite obtained from experimental test and theoretical calculation (Maxwell, and Log mixing rule) at 10 MHz and 20 °C.

4.4.2.5 Mechanical Properties

Touch sensor for used as piezoelectric touch screen require high mechanical properties for their long term operation and tolerance to the applied force during operation. Here, Young's modulus, tensile strength, and elongation at break were measured with universal testing and results are given in Figure 4.19, 4.20, and 4.21, respectively. Loading of MCC at low content was effective for improving the Young's modulus and Tensile strength of PVDF-HFP. The Young's modulus which measures the stiffness of the film was dramatically improved from initial 649 to 1065 MPa in transverse direction and from 696 to 1168 MPa in machine direction for 10 wt.% MCC content. This outstanding property may be attributed to the formation of a networked structure above percolation threshold which was produced by MCC interactions through hydrogen bonding and attributed to the stiff nature of the MCC dispersed [33]. Furthermore, the tensile strength of the composites also increases. The maximum strength was 31 MPa in transverse direction and 53 MPa in machine direction with 5 wt.% loading of MCC. These results further confirm the presence of strong interfacial interaction and good dispersion of MCC in the PVDF-HFP matrix [37]. On the other hand, it was found that high loading of MCC content (20 wt.%) reduce the Young's modulus and Tensile strength. This may be due to the aggregation of MCC, which induced the stress concentration and cracking. The flexibility of PVDF-HFP matrix is reduced when MCC is added and the elongation drops from 285% to 31% in transverse direction when the MCC content is 20 wt.%. There is no obvious decrease in the elongation at break in machine direction with increasing MCC content because MCC are good orientation in machine direction as observed in an optical microscope image.

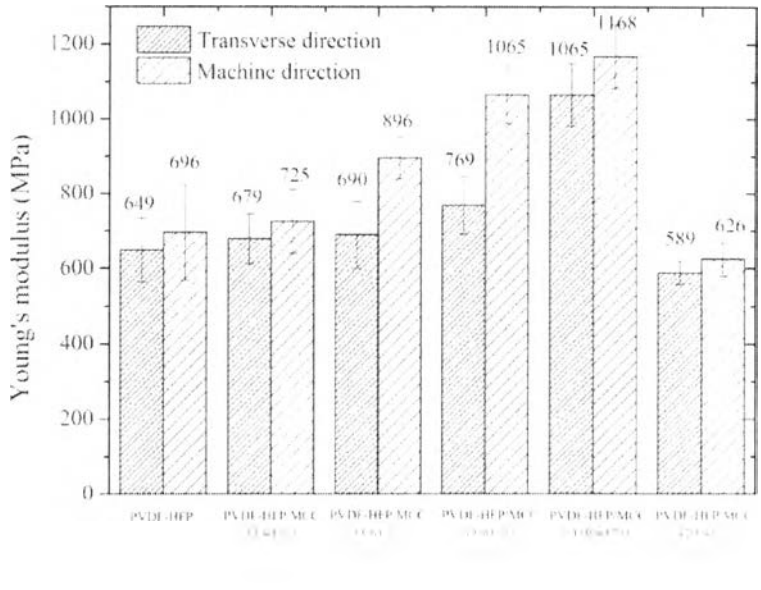

Figure 4.19 Young's modulus of neat PVDF-HFP and composite films.

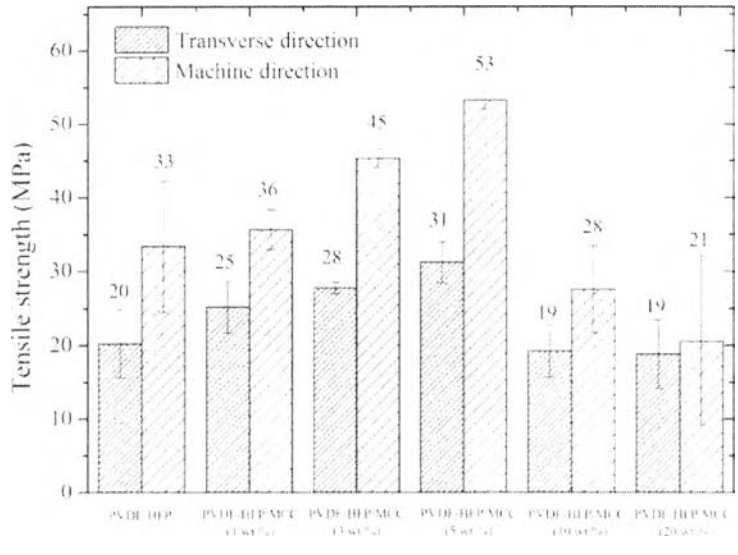

Figure 4.20 Tensile strength of neat PVDF-HFP and composite films.

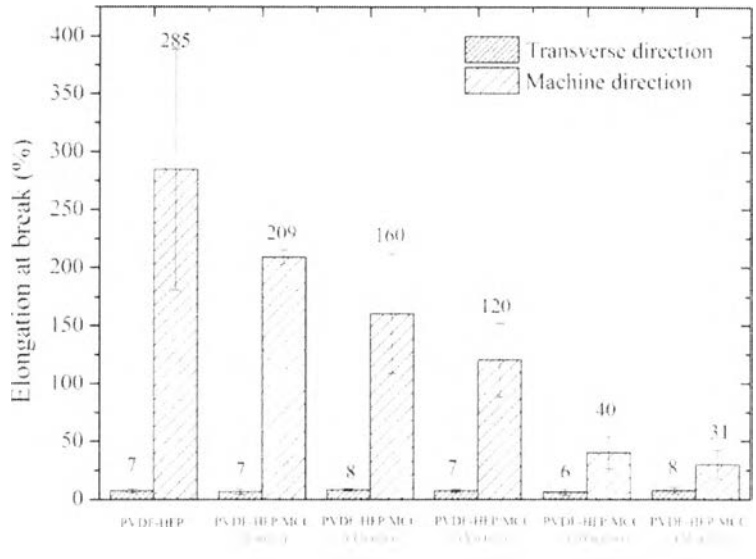

Figure 4.21 Elongation at break of neat PVDF-HFP and composite films.

4.4.2.6 Thermal shrinkage

Thermal shrinkage at high temperature causes the internal short circuit, measuring the thermal shrinkage is very important to evaluate the dimensional thermal stability of the touch sensor. The neat PVDF-HFP and PVDF-HFP/MCC composite film were annealed at 130 °C for 2 hours to further compare their thermal stability at high temperatures. The dimensional changes of neat PVDF-HFP film in the machine direction is 5% and no shrinkage happens in the transverse direction. For high MCC content (5-20 wt.%), no dimensional changes can be observed at 130 °C, indicating excellent dimensional thermal stability because the excellent dimensional stability of MCC at high temperatures makes it promising for the application in high temperature.

4.5 Conclusion

The PVDF-HFP reinforced with microcrystalline cellulose (MCC) at different weight percent, ranging from 1 to 20 wt.%, were successfully prepared by using melt mixing method follow by cast film process. The structure and morphology of the films were studied using SEM. The existences of MCC in the composite films

were confirmed by the analysis of FTIR, TGA, DSC, and XRD. The PVDF-HFP/MCC composite film had appealing feature of optical transparency, high thermal properties, and dielectric properties in term of dielectric constant, which corresponded to piezoelectric coefficient was improve from 2.0 to 3.7 (at 10 MHz) with the addition of 20%wt. of MCC. In addition, their Young's modulus and also tensile strength were dramatically increased comparing with neat PVDF-HFP to the property of MCC. These features satisfied the criteria for the touch sensor application. The PVDF-HFP/MCC composite film containing 10 wt.% MCC was found to have the optimum electrical properties because it was the highest dielectric constant was observed at this MCC content.

4.6 Acknowledgement

This research work was partially supported by the Petroleum and Petrochemical College, Chulalongkorn University, the Ratchadapisek Sompoch Endowment Fund (2013), Chulalongkorn University (CU-56-900-FC), and Thailand Research Fund (IRG5780012).

4.7 Reference

[1] Vatani, M., Engeberg, E.D., and Choi, J.W. (2014) Conformal direct-print of piezoresistive polymer/nanocomposites for compliant multi-layer tactile sensors. Additive Manufacturing.

[2] Kim, D.K., Kim, J.H., Kwon, H.J., and Kwoi, Y.H. (2010) A Touchpad for force and location sensing. ETRI J, 32, 722–8.

[3] Petropoulos, A., Kaltsas, G., Goustouridis, D., and Gogolides, E. (2009) A flexible capacitive device for pressure and tactile sensing. Procedia Chemistry, 1, 867-870.

[4] Dargahi, J. (1998). Piezoelectric and pyroelectric transient signal analysis for detecting the temperature of an object for robotic tactile sensing. Sensor and Actuators A : Phvsical, 71, 89–97.

[5] Harsanyi, G. (2000) Polymer films in sensor applications: a review of present uses and future possibilities. Sensor Review, 20, 98–105.

[6] Wang, T.T., Herbert, J.M., and Glass, A.M. (1988) The Applications of Ferroelectric Polymers. Blackie Publishing, 1, 74-75.

[7] Dargahi, J. and Najarian, S. (2004) International Journal of Medical Robotics and Computer. Assisted Surgery, 1(1), 23–35.

[8] Nalwa, H.S. (1995) Ferroelectric Polymers-Chemistry. Physics and Applications, Marcel Dekker Inc., New York, 203–214.

[9] Salimi, A. and Yousefi, A.A. (2003) FTIR studies of β-phase crystal formation in stretched PVDF films. Polymer Testing, 22(6), 699-704.

[10] Sencadas, V., Moreira, V.M., Lanceros-Méndez, S., Pouzada, A.S., and Gregorio, R. (2006) Alpha-to-beta transformation on PVDF films obtained by uniaxialstretch. Materials Science Forum, 514, 872-876.

[11] Sencadas, V., Gregorio, Jr. R., and Lanceros-Méndez, S. (2008) Alpha to betaphase transformation and microestructural changes of PVDF filmsinduced by uniaxial stretch. Journal of Macromolecular Science, 48, 514-525.

[12] Pan, H., Na, B., Lv, R., Li, C., Zhu, J., and Yu, Z. (2012). Polar phase formation inpoly(vinylidene fluoride) induced by melt annealing. Journal of Polymer Science Part B: Polymer Physics, 50, 1433-1437.

[13] Hattori, T., Kanaoka, M., and Ohigashi, H. (1996) Improved piezoelectricity in thicklamellar beta-form crystals of poly(vinylidene fluoride) crystallizedunder high pressure. Journal of Applied Physics, 79, 2016-2022.

[14] Doll, W.W. and Lando, J.B (1970) Polymorphism of Poly(vinylidene fluoride) Structure of high-pressure-crystallized Poly(vinylidene fluoride). Journal of Macromolecular Science Part B, 4, 89-96.

[15] Ribeiro, C., Sencadas, V., Gomez, J.L., and Lanceros-Méndez, S. (2010) Influ-ence of processing conditions on polymorphism and nanofibermorphology of electroactive poly(vinylidene fluoride) electrospunmembranes. Soft Mater, 8, 274-287.

[16] Czaja, W., Romanovicz, D., and Brown, J.R. (2004) Structural investigations of microbial cellulose produced in stationary and agitated culture. Cellulose, 11, 403-411.

[17] Marcovich, N. E., Auad, M. L., Bellesi, N. E., Nutt, S. R., and Aranguren, M. I. (2006) Cellulose Micro/Nanocrystals Reinforced Polyurethane. Journal of Materials Research, 21(4), 870-881.

[18] Tang, C. and Liu, H. (2008) Cellulose nanofiber reinforced poly(vinyl alcohol) composite film with high visible light transmittance. Composites : Part A, 39, 1638-1643.

[19] Jiang, Z., Caroll, B., and Abraham, K. M. (1997) Electrochim Acta, 42, 2667.

[20] O-Rak, K., Phakdeepataraphan, E., Bunnak, N., Ummartyotin ,S., Sain, M., and Manuspiya, H. (2014) Development of bacterial cellulose and poly(vinylidene fluoride) binary blend system : Structure and properties. Chemical Engineering Journal, 237, 396-402.

[21] Halib, N., Iqbal, M. C., Amin, M., and Ahmad, I. (2012) Physicochemical properties and characterization of Nata de Coco from local food industries as a source of celluose. Sains Malaysiana, 42(2), 205-211.

[22] George, J., Sajeevkumar, V.A., Kumar, R., Ramana, K.V., Sabapathy, S.N., and Bawa, A.S. (2007) Enhancement of thermal stability associated with the chemical treatment of bacterial (gluconacetobacter xylinus) cellulose. Journal of Applied Polymer Science, 108(3), 1845-1851.

[23] Alvarez, C. and Zhang, Z. (2013) Alkaline hydrogen peroxide pretreatment of softwood: Hemicellulose degradation pathways. Bioresource Technology, 150, 321-327.

[24] Valentini, L., Bon, S.B., Cardinali, M., Fortunati, E., and Kenny, J.M. (2014) Cellulose nanocrystals thin films as gate dielectric for flexible organic field-effect transistors. Materials Letters, 126, 55-58.

[25] Sutarlie, L. and Yang, K.L. (2013) Hybrid cellulose aggregate with a silica core for hydrolysis of cellulose and biomass. Journal of colloid and Interface Science, 411(1), 76-81.

[26] Salimi, A. and Yousefi, A.A. (2004) Conformational changes and phase transformation mechanisms in PVDF solution-cast films. Journal of Polymer Science: Part B: Polymer Physics, 42(18), 3487-3495.

[27] Dahan, R.M., Ismail, S.I., Latif, F., Sarip, M.N., Wahid, M.H., and Arshad, A.N. (2012) Dielectric properties of collagen on plasma modified polyvinylidene fluoride. Journal of Applied Sciences, 9(5), 694.

[28] Chang, W.Y., Fang, T.H., Liu, S.Y., and Lin, Y.C. (2008) Phase transformation and thermomechanical characteristics of stretched polyvinylidene fluoride. Materials Science and Engineering A, 480, 477-482.

[29] Chae, D.W., Hwang, S.S., Hong, S.M., Hong, S.P., Cho, B.G., and Kim, B.C. (2007) Influence of high contents of silver nanoparticles on the physical properties of poly(vinylidene fluoride). Molecular crystals and liquid crystals, 464(1), 233-241.

[30] Rao, V., A, P.V., and A, J.V. (2002) Studies on dielectric relaxation and AC conductivity of cellulose acetate hydrogen phthalate-poly(vinyl pyrrolidone) blend. Journal of Applied Polymer Science, 86, 1702-1708.

[31] Linares, A. and Acosta, J.L. (1995) Pyro-piezoelectrics polymers materials. I. Effect of addition of PVA and/or PMMA on overall crystallization kinetics of PVDF from isothermal and non-isothermal data. European Polymer, 31, 615-619.

[32] Ummartyotin, S., Bunnak, N., Juntaro, J., Sain, M., and Manuspiya, H. (2012) Synthesis of colloidal silver nanoparticle for printed electronic. ComptesRendusChimie, 15(6), 539-544.

[33] Costa, P., Silva, J., Sencadas, V., Costa, C.M., Van-Hattum, F.W., and Rocha, J.G. (2009) Carbon, 47, 2590.

[34] Peng, Q.Y., Cong, P.H., Liu, X.J., Liu, T.X., Huang, S., and Li, T.S. (2009) Wear, 266, 713.

[35] Hellinckx, S. and Bauwens, J.C. (1995) Colloid Polym Sci, 273, 219.

[36] Kawai, H. (1969) The piezoelectricity of poly(vinylidene fluoride). Japanese Journal of Applied Physics, 8, 975-976.

[37] Patro, T.U., Mhalgi, M.V., Khakhar, D.V., and Misra, A. (2008) Studies on poly(vinylidene fluoride)–clay nanocomposites:Effect of different clay modifiers. Polymer, 49(16), 3486-3499.